Comparative miRNA Transcriptomics of Mouse and Macaque Reveals MYOC is An Inhibitor for *C. neoformans* Invasion into Brain

Hailong Li[a], Xiaoxu Han[a], Wei Du[b], Yang Meng[b], Yanjian Li[b], Tianshu Sun[c,d], Qiaojing Liang[b], Chao Li[b], Chenhao Suo[b], Xindi Gao[b], Yu Qiu[a], Wen Tian[a], Minghui An[a], Hui Zhang[a], Yajing Fu[a], Xiaolin Li[a], Tian Lan[b], Sheng Yang[b], Zining Zhang[a], Wenqing Geng[a], Chen Ding[b*], Hong Shang[a*]

[a] NHC Key Laboratory of AIDS Immunology (China Medical University), National Clinical Research Center for Laboratory Medicine, The First Affiliated Hospital of China Medical University, Shenyang, 110001, China

[b] College of Life and Health Sciences, Northeastern University, Shenyang, China

[c] Medical Research Centre, State Key Laboratory of Complex Severe and Rare Diseases, Peking Union Medical College Hospital, Chinese Academy of Medical Science, Beijing, China

[d] Beijing Key Laboratory for Mechanisms Research and Precision Diagnosis of Invasive Fungal Diseases, Beijing, China

***Correspondence:**

Hong Shang

hongshang100@hotmail.com

Chen Ding

dingchen@mail.neu.edu.cn

Abstract

Cryptococcal meningoencephalitis is an emerging infection shifted from primarily ART- naive to being ART-experienced HIV/AIDS patients, COVID-19 patients and also in immune competent individuals, mainly caused by the human opportunistic pathogen *Cryptococcus neoformans*, yet mechanisms of the brain or CNS dissemination remain to elucidate, which is the deadest process for the disease. Meanwhile, illustrations of clinically relevant responses in cryptococcosis were limited, as the low availabilities of clinical samples. In this study, macaque and mouse infection models were employed and miRNA-mRNA transcriptomes were performed and combined, which revealed cytoskeleton, a major feather in HIV/AIDS patients, was a centric pathway regulated in both two infection models. Notably, assays of clinical immune cells confirmed an enhanced “Trojan Horse” in HIV/AIDS patients, which can be shut down by cytoskeleton inhibitors. Furthermore, we identified a novel enhancer for macrophage “Trojan Horse”, myocilin, and an enhanced fungal burden was achieved in brains of MYOC transgenic mice. Taking together, this study reveals fundamental roles of cytoskeleton and MYOC in blocking fungal CNS dissemination, which not only helps to understand the high prevalence of cryptococcal meningitis in HIV/AIDS, but also facilitates the development of novel drugs for therapies of meningoencephalitis caused by *C. neoformans* and other pathogenic microorganisms.

Keywords: Cryptococcal meningoencephalitis; HIV/AIDS; Brain dissemination; Host-pathogen interactions; Macaque; miRNA transcriptome; Cytoskeleton; MYOC

Introduction

Fungal invasive diseases are an increasing threat to global public health, lead to more than one million deaths every year, mainly caused by species of *Candida albicans*, *Aspergillus fumigates* and *Cryptococcus neoformans*. Cryptococcal meningoencephalitis (CM) was the leading diseases among fungal meningoencephalitis, caused 181,000 deaths annually, with mortality rates of 100% if untreated[1]. Recent studies showed that the prevalence and mortality has not been decreased, and the appeals for actions on CM was raised[2,3]. Additionally, CM is a major risk for HIV/AIDS patients with 77%-90% prevalence, leading to about 15% deaths of HIV/AIDS patients annually[4]. In the era of ART (antiretroviral therapy), CM is also an emerging infectious disease, shifted from primarily ART- naive to more than 50% being ART-treated[2]. Seriously, morbidity of cryptococcosis in immune competent is increasing rapidly in China, Australia, Canada, and other countries and regions[4-8]. Importantly, COVID-19 patients suffered from secondary cryptococcus infections, suggesting cryptococcosis is an important issue in the post-COVID-19 era [9-12]. Fungal central nervous system (CNS) dissemination is the lethal procedure, which is vital for both fungal colonization and fungal clearance, but lack of mechanisms from in vivo or clinical studies.

To date, massive researches have focused on CNS invasion during fungal meningitis and numerous milestones achieved, including the facts that cryptococci interact with brain epithelial cells directly and indirectly by microscopy or electron microscope[13-16]. These researches are mainly performed on cell lines, mice, zebra fish or rabbits[17], However, clinically relevant evidences were limited, as the unavailability of clinical samples. Cryptococcal meningoencephalitis are predominant prevalent among immune compromised patients, especially HIV/AIDS patients [18-20]. Mechanisms from clinical HIV/AIDS patients were the most direct approach to cryptococcus meningoencephalitis. Dysfunctional cytoskeleton of immune cell was one of pathological features in HIV/AIDS patients[21]. Meanwhile, previous studies indicated that *C. neoformans* infections also disturbed cytoskeleton pathways in mice and human brain microvascular endothelial cells[22,23]. No evidence has revealed the mechanisms between dampened cytoskeleton and

cryptococci brain dissemination. Identification relationships between the cytoskeleton and fungal infections may provide novel mechanisms of fungal pathogenesis and targets for drug development in mycosis.

Furthermore, responses of hosts during infectious diseases are often divided into DNA, mRNA and protein levels, and also, the processes of post transcriptional and translational modifications[22,24,25]. Previous studies identified many responses at mRNA, protein and post translational levels, including key pathways and modulators, such as mineral metabolism, IL-17 signaling pathway, sugar metabolisms, OCSTAMP, IL-5, IL-13 and IL-17A [22,24,26-31]. Post transcriptional modifications, assumed by miRNAs, also play important roles in mRNAs and proteins biosynthesis. Recently, several studies have demonstrated key functions of non-coding RNAs during *C. neoformans* infections in vitro, However, little was known in vivo[32-35].

In this study, to mimic human responses, macaques were employed, and in vivo miRNA-mRNA network was constructed. We found that cytoskeleton pathway is the core pathway regulated by *C. neoformans* in both macaque and mice. Moreover, assays of clinical immune cells confirmed an enhanced “Trojan Horse” in HIV/AIDS patients, and intervention of cytoskeleton pathway was able to disturb “Trojan Horse”. Furthermore, cytoskeleton associated gene, *MYOC*, were identified as important factors for “Trojan Horse” by THP-1 cells and transgenic mice. Collectively, these findings demonstrate global responses at miRNA-mRNA regulatory level, reveal novel modulators for fungal invasion and benefit novel therapies for fungal infectious diseases.

Materials and Methods

Ethics statement

All work with human cells was reviewed and approved by the Medical Research Ethics Committee of the First Affiliated Hospital of China Medical University (2021-63-2). Animal infection experiments in macaques and mice were reviewed and ethically approved by the Research Ethics Committees of the College of Life and Health Sciences of Northeastern University (16099M) and Wincon TheraCells Biotechnologies Co., Ltd. (WD-20150701-a). All animal experiments were carried out according to the Guide for the Care and Use of Laboratory Animals issued by the Ministry of Science and Technology of the People's Republic of China.

Animal Infection

Macaques and mice were purchased from Grandforest Co., Guangxi, China and Changsheng Biotech, China, respectively, and infections were performed same to the previous article[22]. Briefly, six female macaques were divided into two groups. Monkeys were anesthetized by ketamine (10 mg/kg) intraperitoneally injection (IP), and then infected via intratracheal injection with 10^8 cells/kg *C. neoformans* H99 cells. Controls were infected using the same volume of PBS. Mice were anesthetized and infected intranasally with 10^5 fungal cells. Macaque and mice were monitored for signs of infection and humanely killed at day 7 or 14 post infections, or used for survival rates detections.

miRNA sequencing and analysis

Total RNA was isolated using TRIzol. Assessments of RNA were done using a NanoDrop 8000 spectrophotometer. Small RNA-seq libraries were prepared by using TruSeq® Small RNA Library Prep Kit according to the manufacturer’s protocol. miRNA libraries construction and sequencing were entrusted to Shanghai Personal Biotechnology Co., Ltd. (China), and then single-end sequencing was conducted by Illumina NextSeq 500 platform. Raw data were obtained, clean and unique reads were mapped to corresponding

133 genomes by bowtie. Expression of miRNAs were identified by using
134 quantifier.pl in Mirdeep2 based on miRBase21. Differentially expressed
135 miRNAs were calculated by DESeq.

136 **Quantitative PCR of miRNAs**

137 Total miRNAs were isolated by miRNeasy Mini Kit (QIAGEN) according to
138 the manufacturer‘s manual. First strand cDNA was synthesized using random
139 oligonucleotides and miRcuRY LNA Univerersal RT microRNA PCR Universal
140 cDNA Synthesis Kit II (EXIQON, USA), U6 was employed as an internal
141 reference. Primers (Table S4) were designed by using miRprimer and the best
142 primer pairs were selected[36]. RT-qPCR was performed by miRcuRY LNA
143 Univerersal RT microRNA PCR Exilent SYBR master mix (EXIQON, USA)) and
144 StepOne Plus.

145 **Histopathology, colony forming units (CFU) and survival rates**
146 **assessments**

147 Lung tissues were collected from macaque and mice, as described
148 previously [22]. For histopathology analyses, tissue samples were fixed with
149 paraformaldehyde, frozen, and processed using a cryostat microtome (CM1850;
150 Leica). Tissue sections of 10 μm in thickness were stained with mucicarmine or
151 hematoxylin/eosin. For CFUs determination, homogenized lung and brain
152 tissues were diluted and plated onto YPD plates and then incubated at 30°C for
153 two days. Colonies were counted and calculated. For survival rates detection,
154 C57BL/6 mice were divided randomly. Body weight was examined. Fifteen
155 percentage decrease of initial body weight was identified physiological endpoint.

156 **Construction of MYOC overexpressed THP-1 cell line and THP-1 derived**
157 **macrophages (TDMs) differentiation**

158 MYOC gene was cloned into pCDH-EF1α-MCS-T2A-Puro plasmid.
159 Lentivirus was packaged by using jetPRIME® DNA & siRNA Transfection
160 Reagent (polyplus) according to instructions. Infections of THP-1 were
161 performed by centrifugation at 1200 × g at 37 °C in 24-well plates for 2h.

162 Screening of puromycin resistance was conducted 72h post transduction for 2
163 weeks at 5 μg·mL^{-1}. TDMs were differentiated for 48h in RPMI-1640 medium
164 (10% FBS) containing 1% penicillin/streptomycin and 250 ng/mL PMA (Sangon
165 Biotech, China).

166 **Human monocytes isolation and monocyte derived macrophages (MDMs)**
167 **induction**

168 PBMC were isolated by Ficoll-Paque PLUS density gradient media (Cytiva).
169 Blood samples were centrifuged in a swing bucket rotor at 400 × g for 30
170 minutes at 25 ºC with acceleration set at 5 and break at zero, and followed by
171 purification in cold PBS for 2 times and centrifuged at 300 × g for 10 minutes at
172 4 ºC with acceleration and break set at 5. 1×10^{6} PBMC were seeded onto 48-
173 well plates in RPMI-1640 media without FBS for 1h to stick monocytes, and
174 fresh RPMI-1640 medium (10% FBS) containing 1% penicillin/streptomycin and
175 50 ng/mL M-CSF was exchanged, and fresh medium was renewed at days 3
176 and 6 during monocytes differentiation. MDMs were ready to use on day 7.

177 **Phagocytosis effectivity, killing and transmigration assessments**

178 MDMs or TDMs were seeded on 48-well plates at 100,000 cells per well
179 24h before fungi interaction. GFP-expressed strains (H99) were incubated
180 overnight at 30 ºC, washed, opsonized by 18B7(1mg·L^{-1}) at room temperature
181 for 30 min. Incubate fungal cells with macrophages in CO_2 incubator overnight
182 at MOI 1:10. Macrophages and fungal cells were washed 5 times with PBS
183 buffer thoroughly and then digested by trypsin. Phagocytosis effectivity was
184 detected by flow cytometry. For killing tests, after fungi and macrophage
185 incubation (24h), supernatant was collected and cells were washed and
186 collected. Total lysates and supernatant were diluted and plated on YPD agar
187 plates and colonies were counted and calculated 48h post incubation at 30°C.
188 Migration of THP-1 and MDMs were performed by trans-well.

189 **Construction of MYOC transgenic mice**

190 MYOC transgenic mice were produced by Beijing View Solid
191 Biotechnology, China. The linear plasmid pCAG-MYOC cut by the *BstEII*

192 restriction enzyme (NEB) was purified, which were injected into zygotes of
193 C57BL/6 mice in M2 media (Millipore) using a FemtoJet micromanipulator
194 (Eppendorf, Germany). Microinjected zygotes were transferred into pseudo
195 pregnant female mice. All mice were maintained in a specific pathogen-free
196 facility. Genotype identification was performed by PCR and sequencing from 2-
197 week-old newborn mice with primers (Table S4). Transgenic mice were mated
198 with wild-type C57BL/6 mice to obtain heterozygous mice and colony
199 expansion.

200 **Bioinformatics Analysis**

201 Targeted genes of miRNAs were predicted using miRWalk 3.0 [37].
202 Regulatory network miRNA-mRNA was constructed by Cytoscape. Gene
203 ontology and KEGG analyses were performed using R version 4.1.2,
204 clusterProfiler v4.2.0, org.Hs.eg.db version 3.14.0, org.Mm.eg.db version
205 3.14.0 packages, and plotted by ggplot2 version 3.3.5. KEGG of miRNAs was
206 performed by using a web-based application named miEAA [38] and plotted by
207 ggplot2. Heatmap of expression was generated by Pheatmap version 1.0.12.
208 Homology analysis was performed based on miRbase search engine database
209 (https://www.mirbase.org/search.shtml).

210 **Statistics and reproducibility**

211 All experiments were performed at least biologically triplicated to ensure
212 reproducibility. Statistics of phagocytosis effectivity, RT-qPCR, CFU were
213 calculated using GraphPad Prism 9.0. An unpaired or paired student *t* test was
214 performed. When the *p*-value was less than 0.05, statistical significance was
215 recognized.

216 **Data and Software Availability**

217 The RNA-seq raw data files have been deposited in NCBI's Gene
218 Expression Omnibus (GEO) with GEO Series accession ID GSE122785
219 previously[22]. Raw data of microRNA-seq was ready and open to researchers
220 and can be provided upon request.

221 **Author Contributions**

H.S. and C.D. conceived the project. H-L.L., X-X.H., W-Q.G. and C.D. designed the study. T.L., S.Y., and C.D. performed the monkey infection experiments. H-L.L., W.D., Y.M. Q-J.L. Y-J.L. and T-S.S. performed mouse infection experiments. H-L.L., X-L.L., M-H.A., Y.Q., H.Z., X-D.G. and Z-N.Z. participated in data analysis. C-H.S. and C.L. performed histopathology staining. H-L.L., W.T. and Y-J.F. performed cell experiments. H-L.L. X-X.H., W-Q.G., C.D., and H.S. composed the manuscript.

230 **Results**

231 **MicroRNA transcriptomics in macaque and mouse during cryptococcal**
232 **pneumonia.**

233 We have previously unveiled responses in macaque and mouse at
234 transcriptional level and identified several regulators and pathways during *C.*
235 *neoformans* infections[22]. To investigate global responses at post
236 transcriptional level, microRNA transcriptomes were performed using lung
237 tissues isolated from macaque and mouse infection models (Figure 1), and
238 miRNA-mRNA network was constructed, which gave a comprehensive
239 response in cryptococcosis clinically relevant.

240 Pathologies of macaque and mouse lung tissues were confirmed by
241 histopathology observations using mucicarmine and hematoxylin/eosin staining,
242 showing the capsular structure *of C. neoformans* (Figure2 A, B). Total RNAs
243 were extracted and miRNA transcriptomes were performed. Total and unique
244 reads from omics were calculated, with a number of more than 10^7 of total read
245 and 10^6 of unique read (Figure S1A). Read number around 22 nucleotides were
246 the most abundant (Figure S1 B, C). The clean read files were used to map the
247 corresponding genome based on species specificity in miRBase21. However,
248 macaque has few miRNA annotations, as which miRNA annotations of humans
249 were employed for macaque. As a result, there are 1038 and 1166 expressed
250 miRNAs in lung tissues from macaques and mice (Table S1). Principal
251 component analyses (PCA) were analyzed by using read number of each
252 detected miRNA, as shown in Figure 2 C, D, both infected and uninfected
253 samples were reproducible. Differentially expressed miRNAs were performed
254 by DESeq. Heatmaps of differentially expressed items were generated, with 32
255 miRNAs (4 down regulation and 28 up regulation) in macaque and 29 (5 down
256 regulation and 24 up regulation) in mouse, shown as two clusters by column
257 (Figure 2 E, F).

258 **Core responses of host derived from miRNA-mRNA Integrative analyses.**

259 To mine and mimic responses in human cryptococcosis extremely,
260 homology analyses were performed (Figure 3A). Eight miRNAs were co-

261 regulated in macaque and mouse during *C. neoformans* infections. Information
262 about the 8 miRNAs were displayed, including IDs, foldchanges and
263 homologous e-values, and RT-qPCRs were performed in mouse for the 8
264 miRNAs, which were consistent with the miRNA-Seq data (Figure 3 B, C, D).

265 Targets of the 8 co-regulated miRNAs were predicted, then mapped to
266 RNA-Seq, and omics of miRNA and mRNA were integrated (Figure S2). The
267 core regulatory target mRNAs, co-regulated by the 8 co-regulated miRNAs,
268 were selected for a mini miRNA-mRNA network, with 233 target mRNAs
269 identified, including OCSTAMP, DC-STAMP, IL17A TNF and LIF, which
270 demonstrated anti-microbial activities (Figure 3E). KEGG and GO analyses
271 were performed of the 8 co-regulated and 223 co-regulated targets (Figure 4,
272 Figure S3, Table S2 and Table S3). KEGG pathways associated immune
273 system, lung diseases, and infectious diseases were significantly enriched in
274 both miRNA and mRNA level, such as TNF signaling pathway, Cytokine-
275 cytokine receptor interaction, Osteoclast differentiation, small cell lung cancer,
276 non-small cell lung cancer and Influenza A (Figure S3). GO analyses identified
277 terms involved cytokine activity, histone, immune cells, monocyte, myeloid
278 leukocyte and cell cycle were significantly varied by *C. neoformans* (Figure 4).
279 Interestingly, actin binding, microtubule and their associated complex, which
280 constitute cytoskeleton system, were highly enriched in GO analyses, including
281 cellular component, molecular function and biological process. These results
282 indicated a potent function of cytoskeleton in cryptococcosis.

283 **"Trojan Horse" was enhanced in HIV/AIDS patients and can be dampened**
284 **by cytoskeleton pathway inhibitor.**

285 Dysfunctional cytoskeleton of immune cell was one of pathological features
286 in HIV/AIDS patients, who are the predominately population for cryptococcal
287 meningoencephalitis. Based on PSM (Propensity Score Matching, PSM), 100
288 HIV patients and 200 healthy individuals were compared, number and
289 percentage of monocytes were significantly enlarged in HIV patients (Figure
290 5B). To reveal the functions of host cytoskeleton during the battle between host
291 and *C. neoformans*, phagocytosis and transmigration of MDMs from 9
292 HIV/AIDS patients and 8 healthy volunteers were compared (Figure 5A). As

293 shown in Figure 5C, effectivities of phagocytosis were enhanced in HIV/AIDS
294 patients, and more interestingly, the lifted MFI indicated more fungal cells were
295 phagocyted or more intracellular proliferation in HIV/AIDS. Transmigration of
296 MDMs has no change between HIV and healthy volunteers (data not shown),
297 but positively correlated to capacities of phagocytosis (Figure 5D).

298 In order to confirm the association of phenomenon from HIV/AIDS patients
299 with cytoskeleton, R10015, a cytoskeleton pathway inhibitor, was employed,
300 which targets LIM Kinase (LIMK) powerfully in cytoskeleton pathway[39]. Based
301 on the growth curve, 14.815 μM was selected (Figure S4A). THP-1 derived
302 macrophages and human monocyte derived macrophages were employed and
303 pre-treated by R10015 for 2h, washed and then incubated with opsonized *C.*
304 *neoformans* overnight. As shown in figures, R10015 inhibited capacities of
305 phagocytosis and migration of macrophages derived from both THP-1 cell lines
306 and primary monocytes from human (Figure 5 E, F and G, H), however, R10015
307 did not affect the killing in TDMs in and MDMs (Figure 5 I, J). These results
308 confirmed the vital roles of cytoskeleton in macrophage "Trojan Horse".

309 **MYOC is an inhibitor for cryptococci brain dissemination by modulating**
310 **macrophage "Trojan Horse"**

311 To identify functions of cytoskeleton during *C. neoformans* infections,
312 genes associated with cytoskeleton were screened, and myocilin was selected,
313 a tubulin binding protein, encoded by MYOC gene, which was one of the centric
314 modulators in miRNA-mRNA regulatory network and down regulated
315 significantly during *C. neoformans* infections in both macaque and mouse
316 (Figure 6 A, B). Meanwhile, MYOC was elevated in HIV/AIDS patients (Figure
317 6C). Previous studies revealed the protein was involved with cell migration and
318 adhesion[40].
319 To explore functions of MYOC, MYOC overexpressed THP-1 cell lines
320 were constructed and mRNA levels of MYOC were quantified by RT-qPCR,
321 which showed a 10-fold induction compared to mock cells (Figure 6D).
322 Phagocytosis, migration and killing of macrophage cells in MYOC gene-edited
323 cell lines were examined (Figure 6 C, E, F, G). Phagocytosis effectivity was
324 increased significantly in TDMs when MYOC was overexpressed (Figure 6E).

325 Killing capacity was also enhanced by MYOC overexpression, as shown in
326 Figure 6G, less lived *C. neoformans* were detected by CFU assays. However,
327 no changes were observed in migration assays (Figure 6F).
328 To evaluate functions of MYOC in vivo, MYOC- transgenic mouse was
329 generated and employed (Figure 6H), which was confirmed by PCR (Figure 6I).
330 Six-eight weeks old mice were used for CFU assessments and survival rates.
331 To our surprise, CFU of brains was enhanced in MYOC transgenic mice, either
332 in male or female groups (Figure 6J), however, lung CFU was decreased in
333 females, while no changes in the male group (Figure 6K). Consistent with CFU
334 assays, MYOC transgenic mice showed reduced survival times compared to
335 wild type mice observed in survival rate tests (Figure 6L, S4B).
336

Discussion

Cryptococcal meningoencephalitis is an emerging disease with high mortality, even under the ART conditions currently, and deserved more attention in post-COVID-19 era [1-3,9-12]. Brain dissemination is the lethal procedure. However clinically relevant mechanisms were limited[13-17]. In this study, we demonstrated the landscape at transcriptional and post transcriptional levels in mouse and macaque infection models, which were employed for mimicking and unveiling responses at miRNA-mRNA regulatory levels in humans. Previously studies indicated mouse was the most used animal model, however, varied from humans a lot, such as the process of immune cells maturation. Our data from *M. fascicularis*, 92.83% sequence identity to human, a little more clinically relevant, may serve as a database for cryptococcosis or mycosis. To investigate core responses during *C. neoformans* infections, miRNA-mRNA combined, GO and KEGG analyses were performed. Eight key miRNAs were identified in our omics, such as miR-146a, miR-223 and miR-155, which were induced in monocytes by co-culture with *C. neoformans* in vitro[32]. We did not focus on the functions of unique miRNAs, and we characterized cytoskeleton pathway as a core regulatory modulator based on enrichment analyses of miRNAs and their targets. Previous studies identified *C. neoformans* disturbed cytoskeleton when interacted with brain endothelial cells[23].

Our data identified the fundamental roles of cytoskeleton during “Trojan Horse” formation, and provided potential targets for novel “orphan drug” development. Studies have indicated the relationship between cytoskeleton and fungal infections[23,41-44]. However, no mechanisms and in vivo studies to conform. Previous studies highlighted important roles of “Trojan horse” by macrophages during fungal CNS invasion, and the processes are cytoskeleton dependent. Studies have demonstrated migration, adhesion and phagocytosis are key features for phagocytes[45]. Our studies illustrated the basic functions of cytoskeleton dynamics on capacities of phagocytosis and migration of macrophages, which can be shut down by cytoskeleton inhibitors, However, small molecule drugs, such as vanadate, cytochalasin D, Y27632 and R10015

369 are mainly toxic to human [23,39,46]. The toxicity involves fundamental roles of
370 innate immunity and acquired immunity of macrophages, NK cell and T cells,
371 who also play important roles during fungal, bacterial and virus infections.
372 Overcoming toxicity of cytoskeletal inhibitors is the main barrier to clinical
373 application.

374 Further analyses revealed that dysfunctional cytoskeleton may account for
375 the high prevalence of cryptococcal meningitis in HIV/AIDS patients. Studies
376 indicated a similar variation of cytoskeleton pathway during HIV infection and
377 *C. neoformans* or *A. fumigates* infections [23,42,43,47,48]. Indeed, *C.*
378 *neoformans* is an environmental yeast globally ubiquitous, and easily
379 accessible for all individuals[49]. However, why do these happen much more in
380 HIV/AIDS? Previous studies suggested the decreased number of CD4 T cell
381 was a high risk, however contradictory to the high prevalence of high level CD4
382 T cells who are ART experienced[50-52]. Another hypothesis is the high
383 exposure to *C. neoformans* environment, but, inconsistent with the low
384 prevalence of other people in the same environment[53]. Our data suggest the
385 dampened cytoskeleton structure maybe the reason. In HIV/AIDS patients,
386 numerous studies have proved cytoskeleton was dampened in immune cells of
387 PBMC[39,48,54], which contributes to fungal cells CNS invasion by “Trojan
388 Horse”. Furthermore, a recent study proved vomocytosis was enhanced by HIV
389 infection in macrophage[55], which process was also regulated by the
390 cytoskeleton.

391 We identified MYOC as a novel modulator for fungal invasion by regulation
392 on macrophages. Our data showed a repression of MYOC in *C. neoformans*
393 infections and a reduction in HIV infections. Myocilin was proved co-localized
394 with microtubules, endoplasmic reticulum (ER), and Golgi apparatus[56,57] and
395 overexpression of MYOC induces a loss of actin stress fibers[58]. Studies
396 showed myocilin promotes cell migration and phagocytic activities of human
397 trabecular meshwork cells[40,59,60]. In our work, overexpressed MYOC in
398 TDMs elevated phagocytic activities and migration, which induced more
399 intracellular cryptococci and enhanced effects of “Trojan Horse”. These
400 indicated MYOC may the effector for cryptococcoses secondary to HIV/AIDS.

401 In conclusion, our findings therefore described global miRNA-mRNA
402 regulatory responses during *C. neoformans* in primate and rodent animal
403 models, which serves as a clinically relevant database for fundamental and
404 clinical research. We highlight the importance of MYOC and cytoskeleton
405 pathways during *Cryptococcus* meningoencephalitis and underscores their
406 critical functions in the formation of “Trojan Horse” (Figure 7). This study
407 provides critical roles of cytoskeleton on fungal CNS invasion, reveals the
408 directly reasons for the high prevalence of cryptococcal meningitis in HIV/AIDS,
409 and facilitates possibilities for novel anti-fungal drugs development.
410

411 **Acknowledgments**

412 The authors would like to thank Pro. Tongbao Liu from Southwest
413 University, China, for kindly providing GFP-labelled *C. neoformans* strain. This
414 research was supported by the CAMS Innovation Fund for Medical Sciences
415 (2019-I2M-5-027 to HS and XH), the China Postdoctoral Science Foundation
416 (2021M693520 to HL), and the National Natural Science Foundation of China
417 (31870140 to CD and 81801989 to TS).

418 **Disclosure statement**

419 No potential conflict of interest was reported by the authors.

420

421 **Reference**

422 1. Iyer KR, Revie NM, Fu C, et al. Treatment strategies for cryptococcal
423 infection: challenges, advances and future outlook. Nat Rev Microbiol.
424 2021 Jul;19(7):454-466.
425 2. Stott KE, Loyse A, Jarvis JN, et al. Cryptococcal meningoencephalitis:
426 time for action. Lancet Infect Dis. 2021 Sep;21(9):e259-e271.
427 3. Mpoza E, Rajasingham R, Tugume L, et al. Cryptococcal Antigenemia
428 in Human Immunodeficiency Virus Antiretroviral Therapy-Experienced
429 Ugandans With Virologic Failure. Clin Infect Dis. 2020 Oct
430 23;71(7):1726-1731.
431 4. Chen M, Xu N, Xu J. Cryptococcus Neoformans Meningitis Cases
432 Among China's HIV-Infected Population may have been Severely
433 Under-Reported. Mycopathologia. 2020 Dec;185(6):971-974.
434 5. MacDougall L, Kidd SE, Galanis E, et al. Spread of Cryptococcus gattii
435 in British Columbia, Canada, and detection in the Pacific Northwest,
436 USA. Emerg Infect Dis. 2007 Jan;13(1):42-50.
437 6. Huang C, Tsui CKM, Chen M, et al. Emerging Cryptococcus gattii
438 species complex infections in Guangxi, southern China. PLoS Negl Trop
439 Dis. 2020 Aug;14(8):e0008493.
440 7. Bielska E, Sisquella MA, Aldeieg M, et al. Pathogen-derived extracellular
441 vesicles mediate virulence in the fatal human pathogen Cryptococcus
442 gattii. Nat Commun. 2018 Apr 19;9(1):1556.
443 8. Fang W, Zhang L, Liu J, et al. Tuberculosis/cryptococcosis co-infection
444 in China between 1965 and 2016. Emerg Microbes Infect. 2017 Aug
445 23;6(8):e73.
446 9. Shen Y, Zheng F, Sun D, et al. Epidemiology and clinical course of
447 COVID-19 in Shanghai, China. Emerg Microbes Infect. 2020
448 Dec;9(1):1537-1545.
449 10. Cafardi J, Haas D, Lamarre T, et al. Opportunistic Fungal Infection
450 Associated With COVID-19. Open Forum Infect Dis. 2021
451 Jul;8(7):ofab016.

452 11. Song G, Liang G, Liu W. Fungal Co-infections Associated with Global
453 COVID-19 Pandemic: A Clinical and Diagnostic Perspective from China.
454 Mycopathologia. 2020 Aug;185(4):599-606.
455 12. Traver EC, Sánchez MM. Pulmonary aspergillosis and cryptococcosis
456 as a complication of COVID-19. Medical Mycology Case Reports. 2022.
457 13. Charlier C, Nielsen K, Daou S, et al. Evidence of a role for monocytes in
458 dissemination and brain invasion by Cryptococcus neoformans. Infect
459 Immun. 2009 Jan;77(1):120-7.
460 14. Santiago-Tirado FH, Onken MD, Cooper JA, et al. Trojan Horse Transit
461 Contributes to Blood-Brain Barrier Crossing of a Eukaryotic Pathogen.
462 mBio. 2017 Jan 31;8(1).
463 15. Scherer AK, Blair BA, Park J, et al. Redundant Trojan horse and
464 endothelial-circulatory mechanisms for host-mediated spread of
465 Candida albicans yeast. PLoS Pathog. 2020 Aug;16(8):e1008414.
466 16. Sorrell TC, Juillard PG, Djordjevic JT, et al. Cryptococcal transmigration
467 across a model brain blood-barrier: evidence of the Trojan horse
468 mechanism and differences between Cryptococcus neoformans var.
469 grubii strain H99 and Cryptococcus gattii strain R265. Microbes Infect.
470 2016 Jan;18(1):57-67.
471 17. Strickland AB, Shi M. Mechanisms of fungal dissemination. Cell Mol Life
472 Sci. 2021 Jan 15.
473 18. Alves Soares E, Lazera MDS, Wanke B, et al. Mortality by
474 cryptococcosis in Brazil from 2000 to 2012: A descriptive
475 epidemiological study. PLoS Negl Trop Dis. 2019 Jul;13(7):e0007569.
476 19. Akaihe CL, Nweze EI. Epidemiology of Cryptococcus and
477 cryptococcosis in Western Africa. Mycoses. 2021 Jan;64(1):4-17.
478 20. Rajasingham R, Smith RM, Park BJ, et al. Global burden of disease of
479 HIV-associated cryptococcal meningitis: an updated analysis. Lancet
480 Infect Dis. 2017 Aug;17(8):873-881.
481 21. Walsh D, Naghavi MH. Exploitation of Cytoskeletal Networks during
482 Early Viral Infection. Trends Microbiol. 2019 Jan;27(1):39-50.
483 22. Li H, Li Y, Sun T, et al. Unveil the transcriptional landscape at the
484 Cryptococcus-host axis in mice and nonhuman primates. PLoS Negl
485 Trop Dis. 2019 Jul;13(7):e0007566.

486 23. Chen SHM, Stins MF, Huang SH, et al. Cryptococcus neoformans
487 induces alterations in the cytoskeleton of human brain microvascular
488 endothelial cells. J Med Microbiol. 2003 Nov;52(Pt 11):961-970.
489 24. Li H, Li Y, Sun T, et al. Integrative Proteome and Acetylome Analyses of
490 Murine Responses to Cryptococcus neoformans Infection. Front
491 Microbiol. 2020;11:575.
492 25. Li Y, Li H, Sui M, et al. Fungal acetylome comparative analysis identifies
493 an essential role of acetylation in human fungal pathogen virulence.
494 Commun Biol. 2019;2:154.
495 26. Holmer SM, Evans KS, Asfaw YG, et al. Impact of surfactant protein D,
496 interleukin-5, and eosinophilia on Cryptococcosis. Infect Immun. 2014
497 Feb;82(2):683-93.
498 27. Muller U, Stenzel W, Kohler G, et al. IL-13 induces disease-promoting
499 type 2 cytokines, alternatively activated macrophages and allergic
500 inflammation during pulmonary infection of mice with Cryptococcus
501 neoformans. J Immunol. 2007 Oct 15;179(8):5367-77.
502 28. Angkasekwinai P, Sringkarin N, Supasorn O, et al. Cryptococcus gattii
503 infection dampens Th1 and Th17 responses by attenuating dendritic cell
504 function and pulmonary chemokine expression in the immunocompetent
505 hosts. Infect Immun. 2014 Sep;82(9):3880-90.
506 29. Marais S, Meintjes G, Lesosky M, et al. Interleukin-17 mediated
507 differences in the pathogenesis of HIV-1-associated tuberculous and
508 cryptococcal meningitis. AIDS. 2016 Jan 28;30(3):395-404.
509 30. Murdock BJ, Huffnagle GB, Olszewski MA, et al. Interleukin-17A
510 enhances host defense against cryptococcal lung infection through
511 effects mediated by leukocyte recruitment, activation, and gamma
512 interferon production. Infect Immun. 2014 Mar;82(3):937-48.
513 31. Wozniak KL, Hardison SE, Kolls JK, et al. Role of IL-17A on resolution
514 of pulmonary C. neoformans infection. PLoS One. 2011 Feb
515 17;6(2):e17204.
516 32. Chen H, Jin Y, Chen H, et al. MicroRNA-mediated inflammatory
517 responses induced by Cryptococcus neoformans are dependent on the
518 NF-kappaB pathway in human monocytes. Int J Mol Med. 2017
519 Jun;39(6):1525-1532.

520 33. Liu M, Zhang Z, Ding C, et al. Transcriptomic Analysis of Extracellular
521 RNA Governed by the Endocytic Adaptor Protein Cin1 of Cryptococcus
522 deneoformans. Front Cell Infect Microbiol. 2020;10:256.
523 34. Zhang L, Zhang K, Fang W, et al. CircRNA-1806 Decreases T Cell
524 Apoptosis and Prolongs Survival of Mice After Cryptococcal Infection by
525 Sponging miRNA-126. Front Microbiol. 2020;11:596440.
526 35. Jin Y, Yao G, Wang Y, et al. MiR-30c-5p mediates inflammatory
527 responses and promotes microglia survival by targeting eIF2alpha
528 during Cryptococcus neoformans infection. Microb Pathog. 2020
529 Apr;141:103959.
530 36. Busk PK. A tool for design of primers for microRNA-specific quantitative
531 RT-qPCR. BMC Bioinformatics. 2014 Jan 28;15:29.
532 37. Sticht C, De La Torre C, Parveen A, et al. miRWalk: An online resource
533 for prediction of microRNA binding sites. PLoS One.
534 2018;13(10):e0206239.
535 38. Kern F, Fehlmann T, Solomon J, et al. miEAA 2.0: integrating multi-
536 species microRNA enrichment analysis and workflow management
537 systems. Nucleic Acids Res. 2020 Jul 2;48(W1):W521-W528.
538 39. Yi F, Guo J, Dabbagh D, et al. Discovery of Novel Small-Molecule
539 Inhibitors of LIM Domain Kinase for Inhibiting HIV-1. J Virol. 2017 Jul
540 1;91(13).
541 40. Kwon HS, Tomarev SI. Myocilin, a Glaucoma-Associated Protein,
542 Promotes Cell Migration Through Activation of Integrin-Focal Adhesion
543 Kinase-Serine/Threonine Kinase Signaling Pathway. Journal of Cellular
544 Physiology. 2011 Dec;226(12):3392-3402.
545 41. Kim JC, Crary B, Chang YC, et al. Cryptococcus neoformans activates
546 RhoGTPase proteins followed by protein kinase C, focal adhesion
547 kinase, and ezrin to promote traversal across the blood-brain barrier. J
548 Biol Chem. 2012 Oct 19;287(43):36147-57.
549 42. Zhang C, Chen F, Liu X, et al. Gliotoxin Induces Cofilin Phosphorylation
550 to Promote Actin Cytoskeleton Dynamics and Internalization of
551 Aspergillus fumigatus Into Type II Human Pneumocyte Cells. Front
552 Microbiol. 2019;10:1345.

553 43. Kanjanapruthipong T, Sukphopetch P, Reamtong O, et al. Cytoskeletal
554 Alteration Is an Early Cellular Response in Pulmonary Epithelium
555 Infected with Aspergillus fumigatus Rather than Scedosporium
556 apiospermum. Microbial ecology. 2021:1-20.
557 44. Johnston SA, May RC. The human fungal pathogen Cryptococcus
558 neoformans escapes macrophages by a phagosome emptying
559 mechanism that is inhibited by Arp2/3 complex-mediated actin
560 polymerisation. PLoS Pathog. 2010 Aug 12;6(8):e1001041.
561 45. Tang DD, Gerlach BD. The roles and regulation of the actin cytoskeleton,
562 intermediate filaments and microtubules in smooth muscle cell migration.
563 Respir Res. 2017 Apr 8;18(1):54.
564 46. Meyerovitch J, Farfel Z, Sack J, et al. Oral administration of vanadate
565 normalizes blood glucose levels in streptozotocin-treated rats.
566 Characterization and mode of action. J Biol Chem. 1987 May
567 15;262(14):6658-62.
568 47. Kogan TV, Jadoun J, Mittelman L, et al. Involvement of secreted
569 Aspergillus fumigatus proteases in disruption of the actin fiber
570 cytoskeleton and loss of focal adhesion sites in infected A549 lung
571 pneumocytes. J Infect Dis. 2004 Jun 1;189(11):1965-73.
572 48. He S, Fu Y, Guo J, et al. Cofilin hyperactivation in HIV infection and
573 targeting the cofilin pathway using an anti-alpha4beta7 integrin antibody.
574 Sci Adv. 2019 Jan;5(1):eaat7911.
575 49. Montoya MC, Magwene PM, Perfect JR. Associations between
576 Cryptococcus Genotypes, Phenotypes, and Clinical Parameters of
577 Human Disease: A Review. J Fungi (Basel). 2021 Mar 30;7(4).
578 50. Molloy SF, Kanyama C, Heyderman RS, et al. Antifungal Combinations
579 for Treatment of Cryptococcal Meningitis in Africa. N Engl J Med. 2018
580 Mar 15;378(11):1004-1017.
581 51. Meya D, Rajasingham R, Nalintya E, et al. Preventing Cryptococcosis-
582 Shifting the Paradigm in the Era of Highly Active Antiretroviral Therapy.
583 Curr Trop Med Rep. 2015;2(2):81-89.
584 52. Tugume L, Rhein J, Hullsiek KH, et al. HIV-associated cryptococcal
585 meningitis occurring at relatively higher CD4 counts. The Journal of
586 infectious diseases. 2019;219(6):877-883.

587 53. Fisher JF, Valencia-Rey PA, Davis WB. Pulmonary Cryptococcosis in
588 the Immunocompetent Patient-Many Questions, Some Answers. Open
589 Forum Infect Dis. 2016 Sep;3(3):ofw167.
590 54. Yoder A, Yu D, Dong L, et al. HIV envelope-CXCR4 signaling activates
591 cofilin to overcome cortical actin restriction in resting CD4 T cells. Cell.
592 2008 Sep 5;134(5):782-92.
593 55. Seoane PI, Taylor-Smith LM, Stirling D, et al. Viral infection triggers
594 interferon-induced expulsion of live Cryptococcus neoformans by
595 macrophages. PLoS Pathog. 2020 Feb;16(2):e1008240.
596 56. Mertts M, Garfield S, Tanemoto K, et al. Identification of the region in the
597 N-terminal domain responsible for the cytoplasmic localization of
598 Myoc/Tigr and its association with microtubules. Lab Invest. 1999
599 Oct;79(10):1237-45.
600 57. Sohn S, Hur W, Joe MK, et al. Expression of wild-type and truncated
601 myocilins in trabecular meshwork cells: their subcellular localizations
602 and cytotoxicities. Investigative ophthalmology & visual science.
603 2002;43(12):3680-3685.
604 58. Shen X, Koga T, Park BC, et al. Rho GTPase and cAMP/protein kinase
605 A signaling mediates myocilin-induced alterations in cultured human
606 trabecular meshwork cells. J Biol Chem. 2008 Jan 4;283(1):603-612.
607 59. Wentz-Hunter K, Kubota R, Shen X, et al. Extracellular myocilin affects
608 activity of human trabecular meshwork cells. J Cell Physiol. 2004
609 Jul;200(1):45-52.
610 60. Wentz-Hunter K, Shen X, Okazaki K, et al. Overexpression of myocilin
611 in cultured human trabecular meshwork cells. Exp Cell Res. 2004 Jul
612 1;297(1):39-48.
613

614 **Figure legends**

615 **Figure 1. Flow chart for animal infections and RNA sequencing**

616 Six macaques and mice were divided into two groups randomly and infected by
617 H99 intranasally. Lung tissues were isolated 7 days post infections. Total RNAs
618 were isolated for mRNA-seq and miRNA-seq followed by confirmation of
619 histopathology. Differentially expressed miRNA-mRNA regulatory network was
620 constructed. Figure 1 was created with BioRender.com

621 **Figure 2. miRNA-Seq of mice and macaques in response to *C. neoformans***

622 **A B. Histopathology observation of infected macaque and mouse lung**
623 **tissues.** Lung tissues from macaque and mouse were fixed and sectioned at
624 10 μm thickness and stained by using mucicarmine. Red arrows indicate *C.*
625 *neoformans* cells, scale bar = 10 μm.

626 **C D. PCAs of miRNA-Seq data.**

627 **E F. Heatmaps of differentially expressed miRNAs.** miRNAs with *p*-value ≤
628 0.05, fold change≥ 2 were considered as differentially expressed.

629 **Figure 3. Core regulatory machinery of miRNA-mRNA network during *C.***
630 ***neoformans* infections.**

631 **A. Schedule of identification of homologous miRNA.** miRNAs of macaque
632 were used for searching homologous miRNAs in miRbase.

633 **B. Venn diagram of differentially expressed miRNAs.**

634 **C. Information of 8 co-regulated miRNAs.**

635 **D. RT-qPCR of the 8 co-regulated miRNAs in mouse.** Three biological
636 replicates were performed. Mean and SEM were shown. Unpaired student *t* test
637 was performed. *$p < 0.05$, ** $p < 0.01$, or ***$p < 0.005$.

638 **E. miRNA-mRNA core regulatory network.** Differentially expressed target
639 genes of 8 co-regulated miRNAs were shown. The whole network is shown in
640 Figure S3.

641 **Figure 4. GO analyses of co-regulated miRNAs and mRNAs in macaque**
642 **and mouse during *C. neoformans* infections.**

643 **A. GOs of miRNAs calculated by miEAA. B. GOs of target mRNAs**
644 **enriched by Clusterprofiler.** Eight co-regulated miRNAs and co-regulated
645 mRNAs from Figure 4E were employed for GO analyses, respectively. Top 10
646 or all significantly enriched GO terms were plotted. Green, blue and red
647 columns represent cellular component, molecular function and biological
648 process, respectively.

649 **Figure 5. "Trojan Horse" was enhanced in HIV/AIDS patients**

650 **A. Strategies for phagocytosis assessment by flow cytometry**.
651 Cryptococcal internalization was determined by flow cytometry using GFP-
652 expressed H99. During flow cytometry, single cells were selected, cells with
653 negative Uvitex 2B were considered as phagocytes, and in which FITC positive
654 cells were fungi internalized (Uvitex 2B -/ FITC +).

655 **B.** Number and percentage of monocytes between HIV patients and healthy
656 individuals from clinical data

657 **C.** Phagocytosis effectivity of MDMs from HIV patients and healthy individuals

658 **D.** Correlation of phagocytosis and migration in MDMs from HIV patients.

659 **E, F.** Phagocytosis effectivity was inhibited by R10015 in TDMs(E) and MDMs(F)

660 **G, H.** cells migration was dampened by R10015 in THP-1(G) and MDMs(H).

661 **I, J.** R10015 does not affect killing *C. neoformans* in THP-1(I) and MDMs(J).

662 **Figure 6. MYOC enhanced *C. neoformans* brain invasion by modulating**
663 **macrophage "Trojan Horse"**

664 **A.** miRNAs-mRNA network during *C. neoformans* infections.

665 **B.** Normalized MYOC reads in mouse and macaque in response to *C.*
666 *neoformans.*

667 **C.** Intensity of MYOC protein from comparative proteomes between HIV and
668 AIDS patients.

669 **D.** Relative expression level of MYOC in MYOC gene edited THP-1 cell lines.

670 **E. Effectivity of phagocytosis in MYOC overexpressed THP-1 derived**
671 **macrophages by flowcytometry.** Four biological replicates were performed.
672 Unpaired Student *t* test was performed. * $p < 0.05$.

673 **F.** Capacity of migration in MYOC overexpressed THP-1 cell lines.

674 **G.** Killing tests of MYOC overexpressed THP-1 derived macrophages.

675 **H. Photo of MYOC transgenic mice.** The cute picture is one of our MYOC
676 transgenic mice,5-week-old, which showed healthy and eye-functioned.

677 **I. MYOC gene fragment was checked by agarose electrophoresis in MYOC**
678 **transgenic mice.** Genome DNA was isolated and PCR and electrophoresis
679 were performed. Target PCR products was 498 bp.

680 **J, K. CFU assessments of MYOC transgenic mice, brain(J) and lung(K)**
681 **tissues.** Seven MYOC transgenic mice (3 male and 4 female) and 8 wild type
682 mice (4 male and 4 female) from the same cages were used for CFU assays.
683 Unpaired Student *t* test was performed. * $p < 0.05$.

684 **L. Survival tests of MYOC transgenic mice.** Eleven MYOC transgenic mice
685 (5 male and 6 female) and 9 wild type mice (3 male and 6 female) from the
686 same cages were used for survival assays. *Log-rank* (Mantel-Cox) test was
687 employed for statistical analysis. * $p < 0.05$.

688 **Figure 7. Conceptual graph of HIV triggered cryptococcal**
689 **meningoencephalitis**

690 HIV-1 infections trigger cytoskeleton dynamics by induction of MYOC protein,
691 enhance macrophage “Trojan Horse” and induce cryptococcus

692 meningoencephalitis (shown in blue lines). Inhibitions of cytoskeleton pathways
693 or MYOC dampen “Trojan Horse” and decrease the number of cryptococci in
694 the brain (shown in red lines). Figure 7 was created with BioRender.com

695 **Supporting information**

696 **Figure S1. Read number of miRNA-Seq.**

697 **A.** Total and unique read number of miRNA-Seq.

698 **B.** Distribution of different lengths of nucleotides from macaques.

699 **C.** Distribution of different lengths of nucleotides from mice.

700 **Figure S2. Network of miRNA-mRNA during cryptococcal pneumonia.**

701 **Figure S3. KEGG analysis of co-regulated miRNAs and targeted mRNAs.**

702 **Figure S4. Growth curve of *C. neoformans* and body weight loss of mice**
703 **in survival rates.**

704 **A. Growth curve of H99 in different concentrations of R10015**.

705 **B. Body weight of mice**. Blue line indicated wild type control group and red
706 line MYOC transgenic mice. Dash dot lines represent 85% of the initial average
707 body weight.

708 **Table S1.** Differentially expressed miRNAs in macaque and mouse lung tissues
709 during *C. neoformans* infections.

710 **Table S2.** GO and KEGG analyses of 8 co-regulated miRNAs in response to
711 *C. neoformans* infections.

712 **Table S3.** GO and KEGG analyses of target genes for co-regulated 8 miRNAs
713 in mouse and macaque.

714 **Table S4.** Primers used in the study.

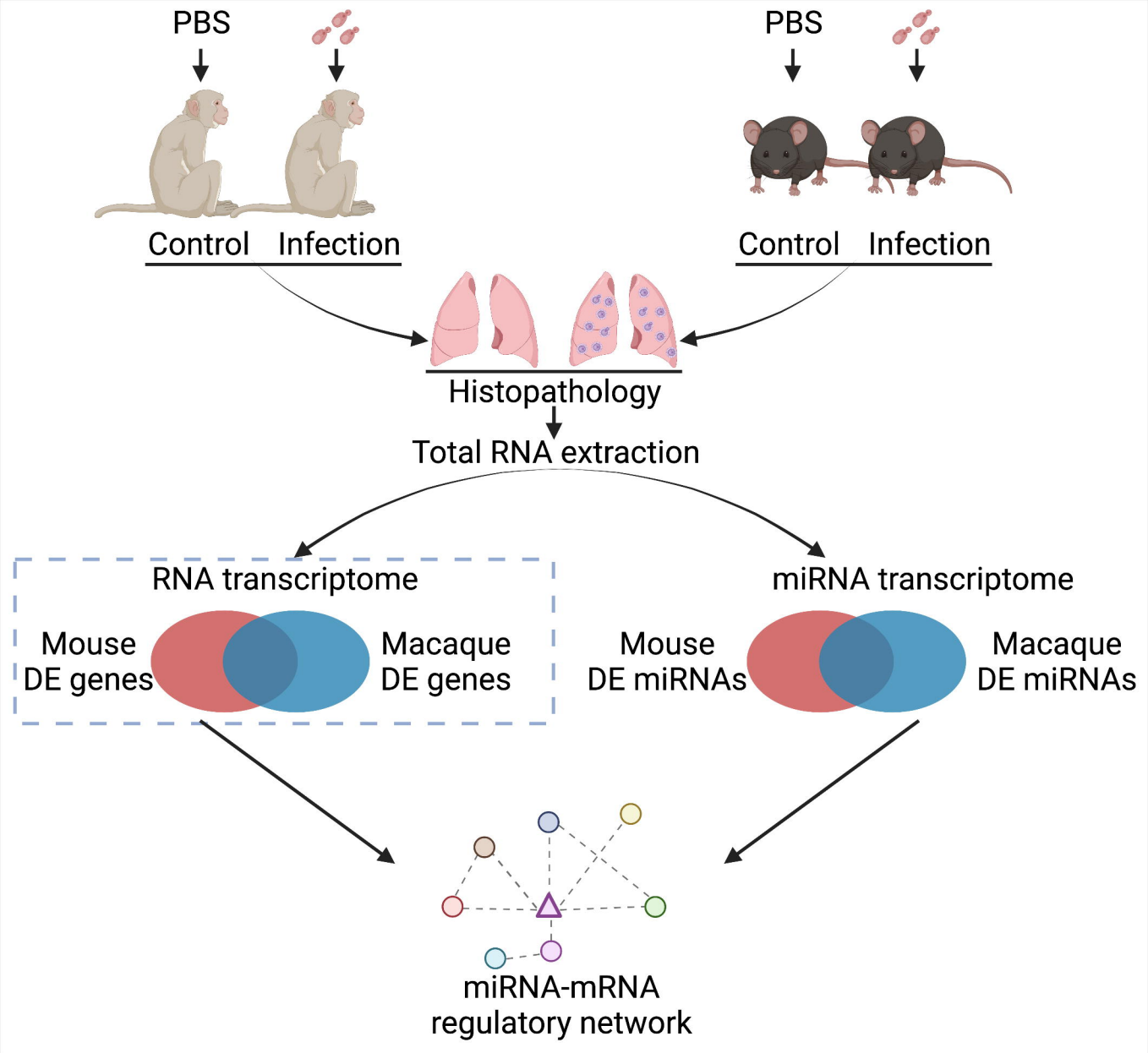
PBS
PBS
Control
Infection
Control
Infection
Histopathology
Total RNA extraction
RNA transcriptome
Mouse
DE genes
Macaque
DE genes
miRNA transcriptome
Mouse
DE miRNAs
Macaque
DE miRNAs
miRNA-mRNA
regulatory network

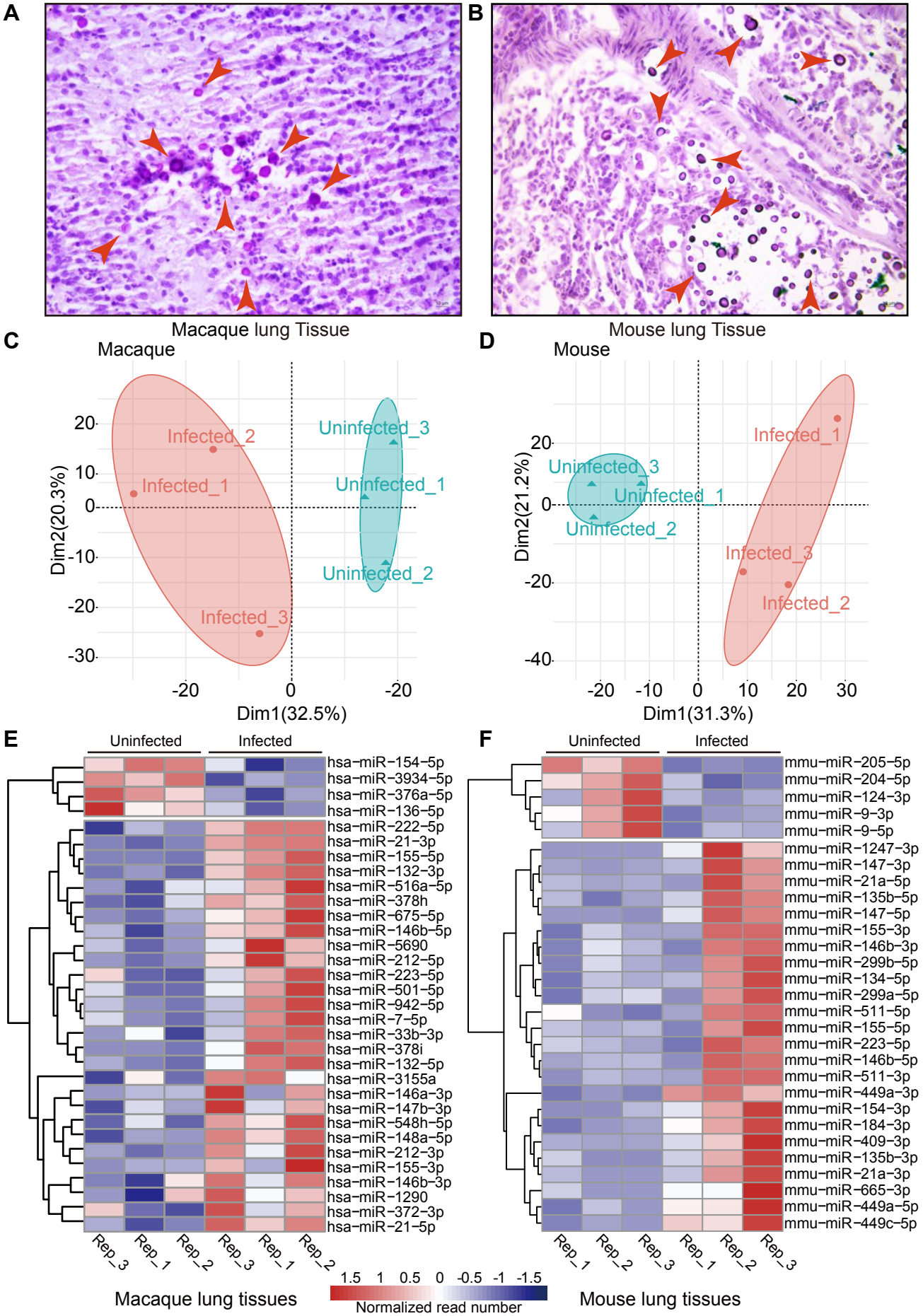
A
B
Macaque lung Tissue
Mouse lung Tissue
C
Macaque
Infected_2
Infected_1
Infected_3
Uninfected_3
Uninfected_1
Uninfected_2
Dim2(20.3%)
Dim1(32.5%)
D
Mouse
Infected_1
Infected_3
Infected_2
Uninfected_3
Uninfected_1
Uninfected_2
Dim2(21.2%)
Dim1(31.3%)
E
Uninfected
Infected
hsa-miR-154-5p
hsa-miR-3934-5p
hsa-miR-376a-5p
hsa-miR-136-5p
hsa-miR-222-5p
hsa-miR-21-3p
hsa-miR-155-5p
hsa-miR-132-3p
hsa-miR-516a-5p
hsa-miR-378h
hsa-miR-675-5p
hsa-miR-146b-5p
hsa-miR-5690
hsa-miR-212-5p
hsa-miR-223-5p
hsa-miR-501-5p
hsa-miR-942-5p
hsa-miR-7-5p
hsa-miR-33b-3p
hsa-miR-378i
hsa-miR-132-5p
hsa-miR-3155a
hsa-miR-146a-3p
hsa-miR-147b-3p
hsa-miR-548h-5p
hsa-miR-148a-5p
hsa-miR-212-3p
hsa-miR-155-3p
hsa-miR-146b-3p
hsa-miR-1290
hsa-miR-372-3p
hsa-miR-21-5p
Rep_3 Rep_1 Rep_2 Rep_3 Rep_1 Rep_2
Macaque lung tissues
F
Uninfected
Infected
mmu-miR-205-5p
mmu-miR-204-5p
mmu-miR-124-3p
mmu-miR-9-3p
mmu-miR-9-5p
mmu-miR-1247-3p
mmu-miR-147-3p
mmu-miR-21a-5p
mmu-miR-135b-5p
mmu-miR-147-5p
mmu-miR-155-3p
mmu-miR-146b-3p
mmu-miR-299b-5p
mmu-miR-134-5p
mmu-miR-299a-5p
mmu-miR-511-5p
mmu-miR-155-5p
mmu-miR-223-5p
mmu-miR-146b-5p
mmu-miR-511-3p
mmu-miR-449a-3p
mmu-miR-154-3p
mmu-miR-184-3p
mmu-miR-409-3p
mmu-miR-135b-3p
mmu-miR-21a-3p
mmu-miR-665-3p
mmu-miR-449a-5p
mmu-miR-449c-5p
Rep_1 Rep_2 Rep_3 Rep_1 Rep_2 Rep_3
Mouse lung tissues
1.5 1 0.5 0 -0.5 -1 -1.5
Normalized read number

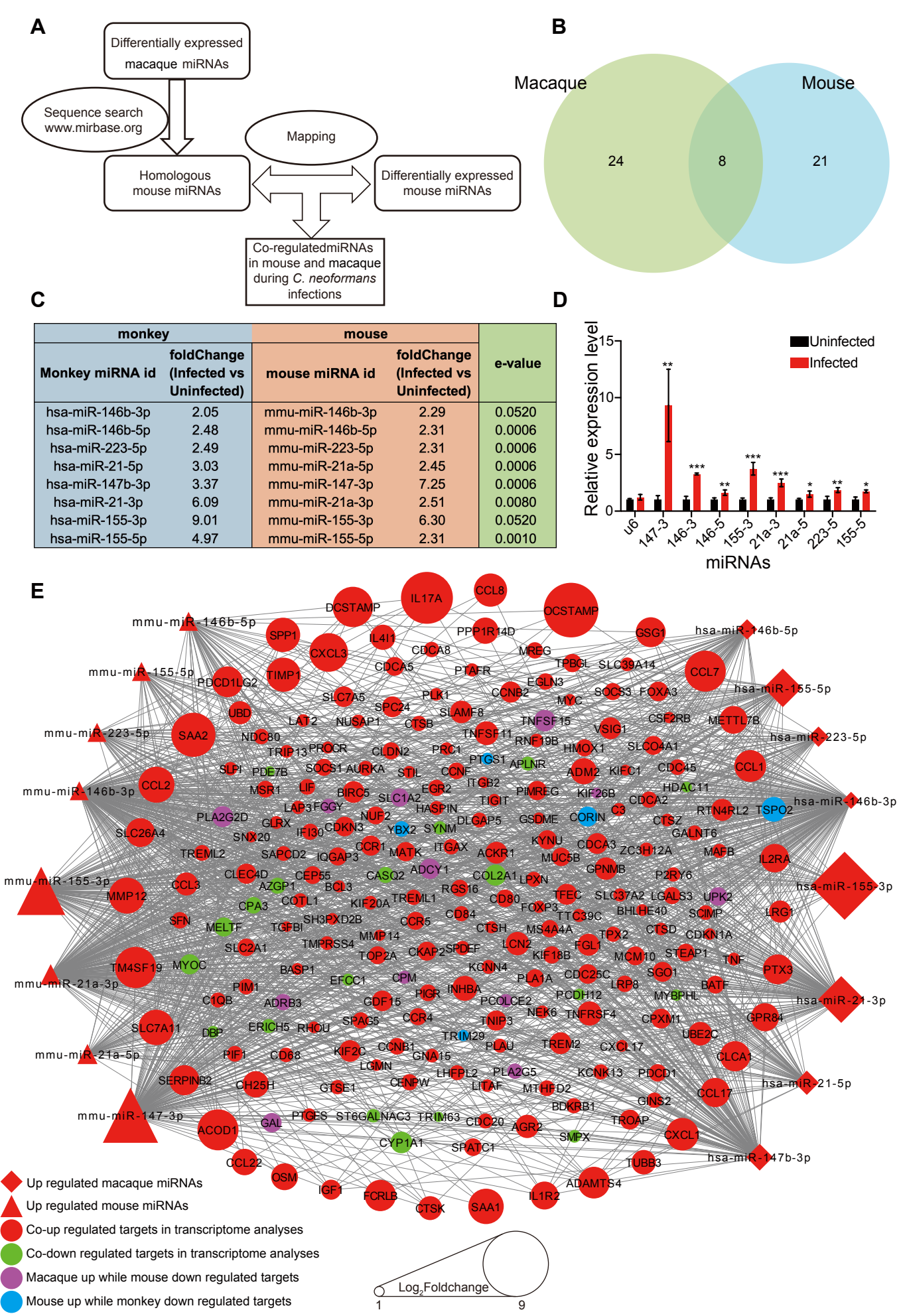

monkey		mouse		e-value
Monkey miRNA id	foldChange (Infected vs Uninfected)	mouse miRNA id	foldChange (Infected vs Uninfected)	
hsa-miR-146b-3p	2.05	mmu-miR-146b-3p	2.29	0.0520
hsa-miR-146b-5p	2.48	mmu-miR-146b-5p	2.31	0.0006
hsa-miR-223-5p	2.49	mmu-miR-223-5p	2.31	0.0006
hsa-miR-21-5p	3.03	mmu-miR-21a-5p	2.45	0.0006
hsa-miR-147b-3p	3.37	mmu-miR-147-3p	7.25	0.0006
hsa-miR-21-3p	6.09	mmu-miR-21a-3p	2.51	0.0080
hsa-miR-155-3p	9.01	mmu-miR-155-3p	6.30	0.0520
hsa-miR-155-5p	4.97	mmu-miR-155-5p	2.31	0.0010

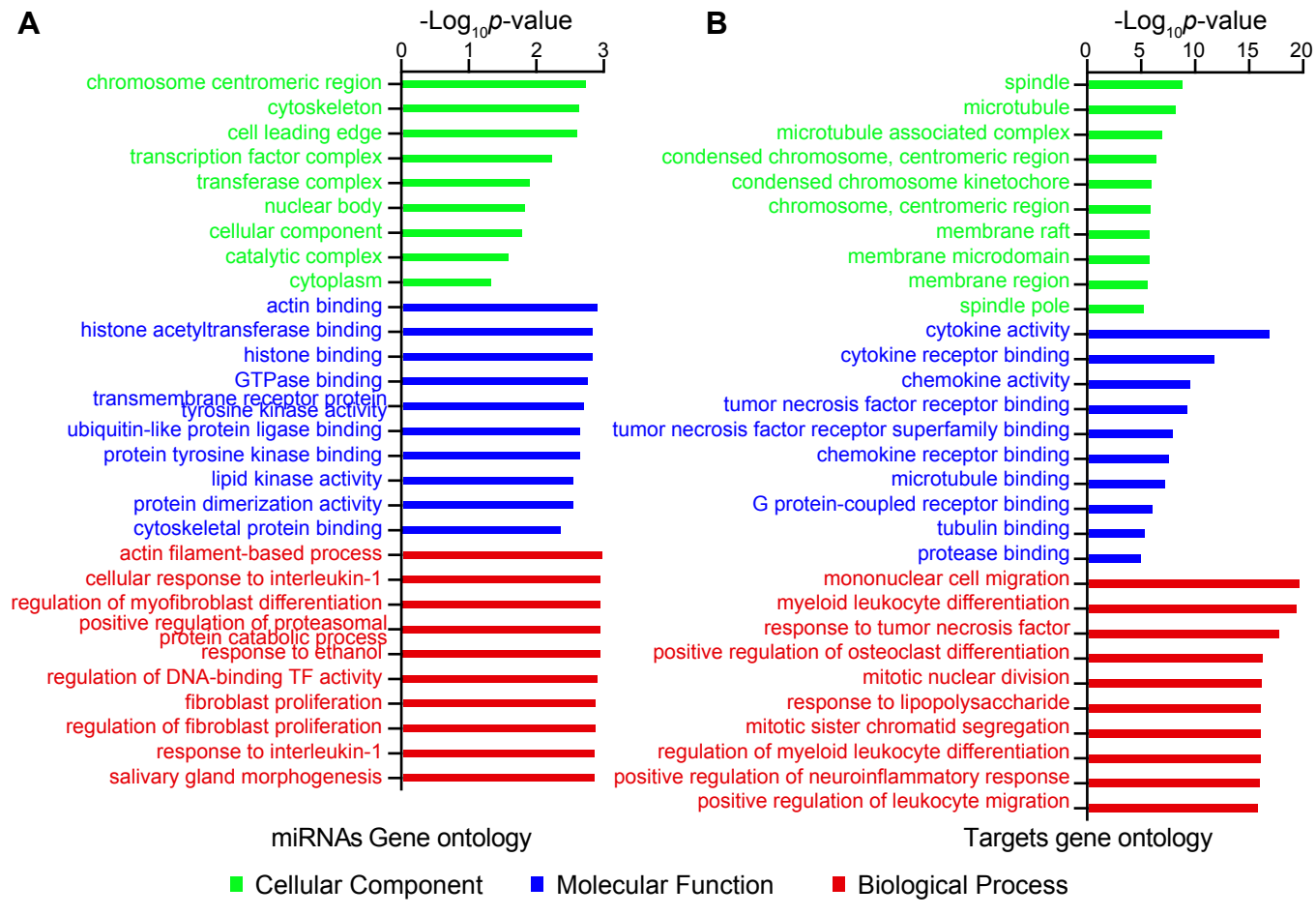
A
-Log10p-value
0
1
2
3
chromosome centromeric region
cytoskeleton
cell leading edge
transcription factor complex
transferase complex
nuclear body
cellular component
catalytic complex
cytoplasm
actin binding
histone acetyltransferase binding
histone binding
GTPase binding
transmembrane receptor protein tyrosine kinase activity
ubiquitin-like protein ligase binding
protein tyrosine kinase binding
lipid kinase activity
protein dimerization activity
cytoskeletal protein binding
actin filament-based process
cellular response to interleukin-1
regulation of myofibroblast differentiation
positive regulation of proteasomal protein catabolic process
response to ethanol
regulation of DNA-binding TF activity
fibroblast proliferation
regulation of fibroblast proliferation
response to interleukin-1
salivary gland morphogenesis
miRNAs Gene ontology
B
-Log10p-value
0
5
10
15
20
spindle
microtubule
microtubule associated complex
condensed chromosome, centromeric region
condensed chromosome kinetochore
chromosome, centromeric region
membrane raft
membrane microdomain
membrane region
spindle pole
cytokine activity
cytokine receptor binding
chemokine activity
tumor necrosis factor receptor binding
tumor necrosis factor receptor superfamily binding
chemokine receptor binding
microtubule binding
G protein-coupled receptor binding
tubulin binding
protease binding
mononuclear cell migration
myeloid leukocyte differentiation
response to tumor necrosis factor
positive regulation of osteoclast differentiation
mitotic nuclear division
response to lipopolysaccharide
mitotic sister chromatid segregation
regulation of myeloid leukocyte differentiation
positive regulation of neuroinflammatory response
positive regulation of leukocyte migration
Targets gene ontology
Cellular Component
Molecular Function
Biological Process

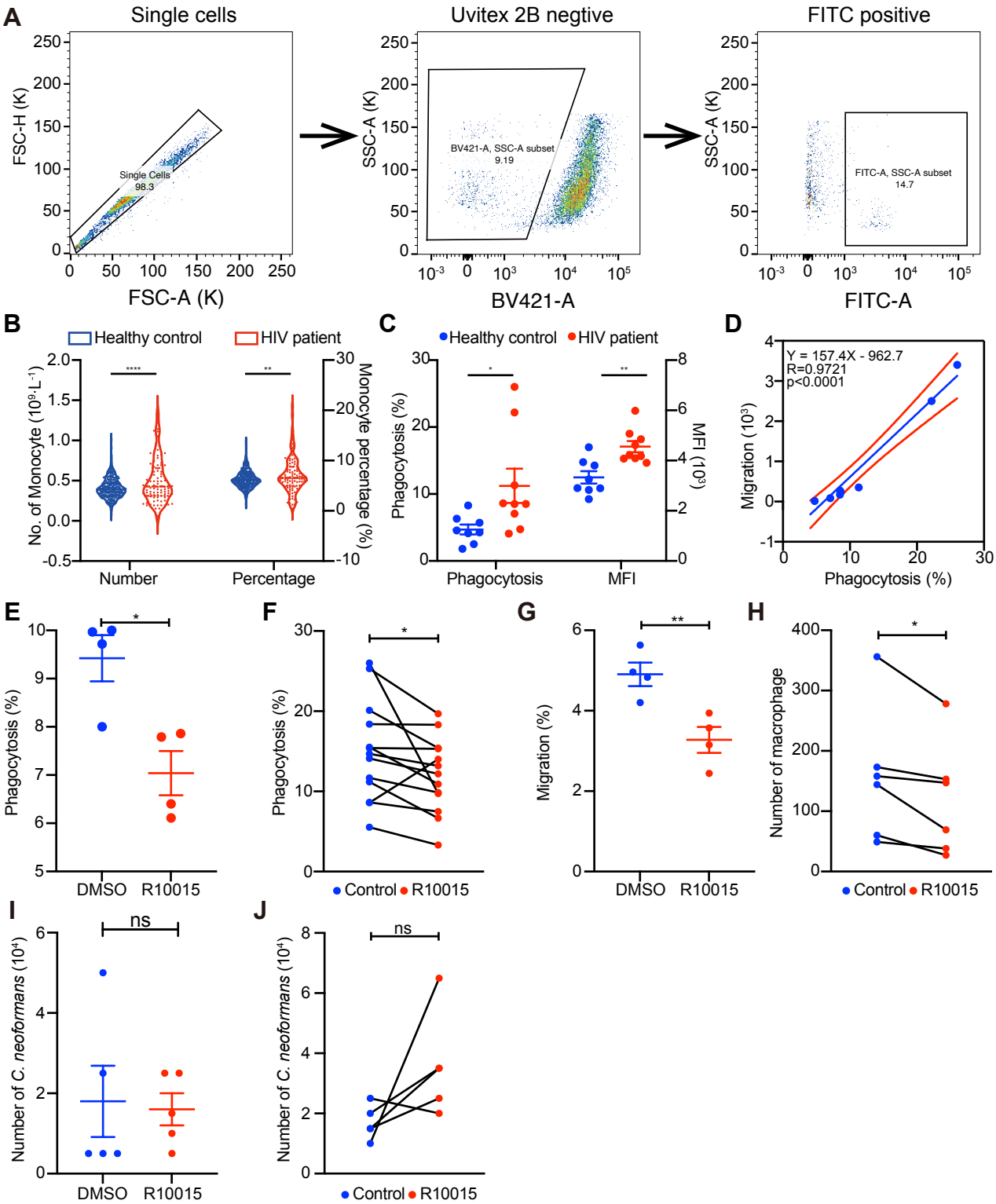
A
Single cells
Uvitex 2B negtive
FITC positive
FSC-H (K)
FSC-A (K)
Single Cells
98.3
SSC-A (K)
BV421-A
BV421-A, SSC-A subset
9.19
FITC-A
FITC-A, SSC-A subset
14.7
B
Healthy control
HIV patient
No. of Monocyte (10⁹·L⁻¹)
Monocyte percentage (%)
Number
Percentage
C
Phagocytosis (%)
MFI (10³)
Phagocytosis
MFI
D
Y = 157.4X - 962.7
R=0.9721
p<0.0001
Migration (10³)
Phagocytosis (%)
E
Phagocytosis (%)
DMSO
R10015
F
Phagocytosis (%)
Control
R10015
G
Migration (%)
DMSO
R10015
H
Number of macrophage
Control
R10015
I
ns
Number of C. neoformans (10⁴)
DMSO
R10015
J
ns
Number of C. neoformans (10⁴)
Control
R10015

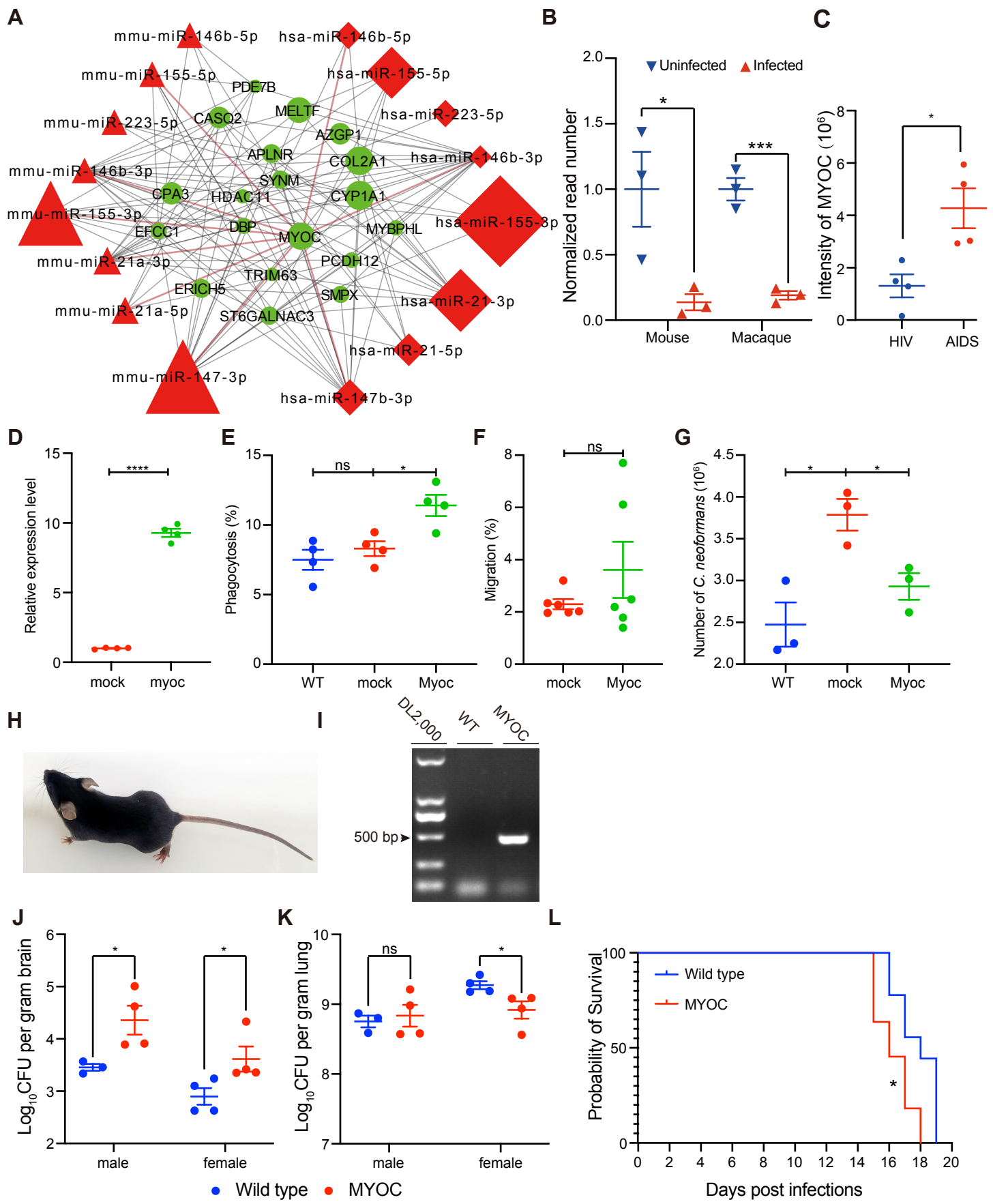
A
mmu-miR-146b-5p
hsa-miR-146b-5p
mmu-miR-155-5p
hsa-miR-155-5p
PDE7B
MELTF
CASQ2
mmu-miR-223-5p
hsa-miR-223-5p
AZGP1
APLNR
COL2A1
hsa-miR-146b-3p
mmu-miR-146b-3p
SYNM
CPA3
HDAC11
CYP1A1
mmu-miR-155-3p
hsa-miR-155-3p
EFCC1
DBP
MYOC
MYBPHL
mmu-miR-21a-3p
PCDH12
TRIM63
ERICH5
SMPX
hsa-miR-21-3p
mmu-miR-21a-5p
ST6GALNAC3
hsa-miR-21-5p
mmu-miR-147-3p
hsa-miR-147b-3p
B
Uninfected
Infected
Normalized read number
Mouse
Macaque
C
Intensity of MYOC (10^6)
HIV
AIDS
D
Relative expression level
mock
myoc
E
Phagocytosis (%)
ns
WT
mock
Myoc
F
Migration (%)
G
Number of C. neoformans (10^6)
H
I
DL2,000
WT
MYOC
500 bp
J
Log10CFU per gram brain
male
female
K
Log10CFU per gram lung
L
Probability of Survival
Wild type
MYOC
Days post infections

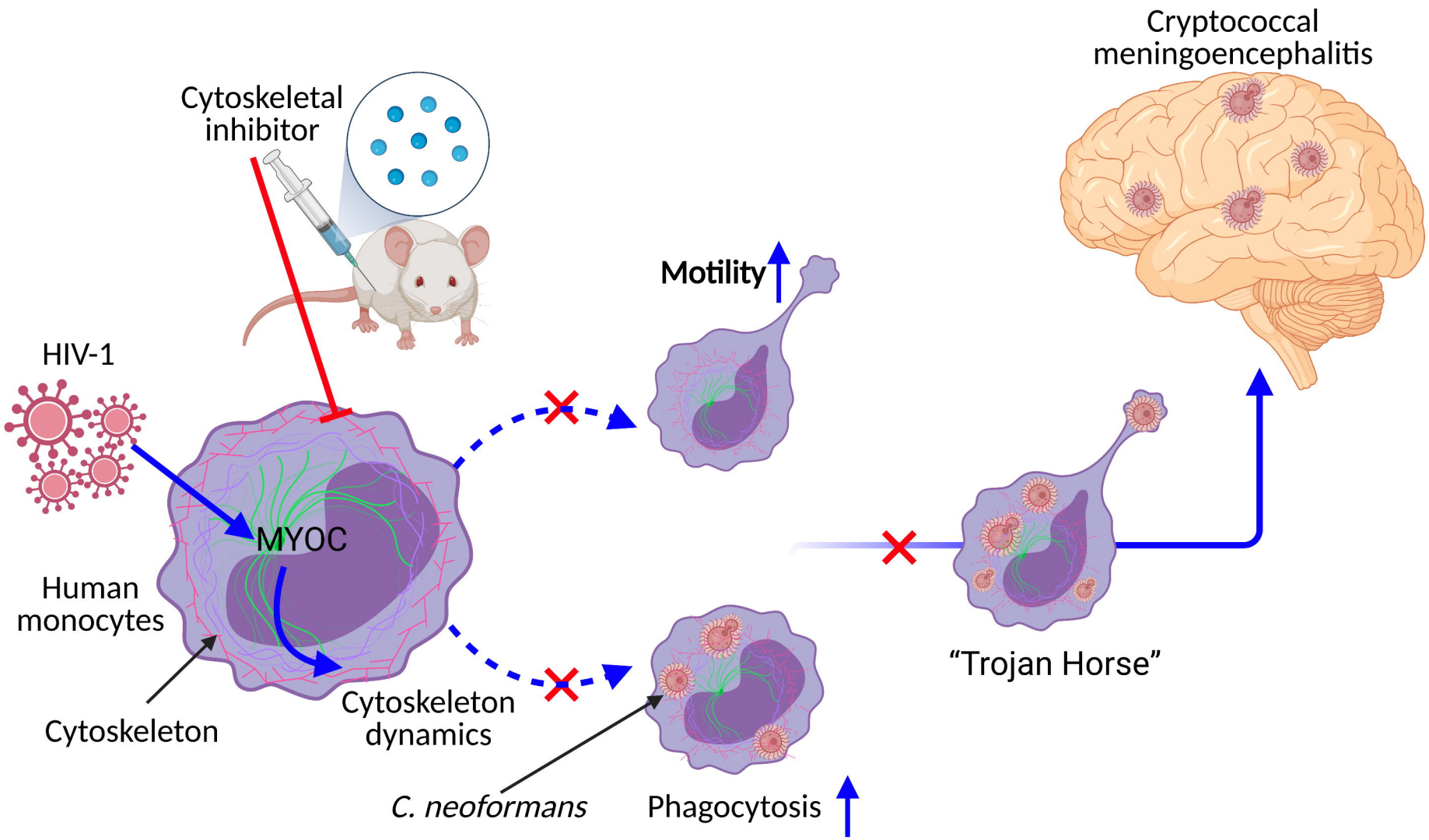
Cryptococcal meningoencephalitis
Cytoskeletal inhibitor
Motility
HIV-1
MYOC
Human monocytes
Cytoskeleton
Cytoskeleton dynamics
"Trojan Horse"
C. neoformans
Phagocytosis

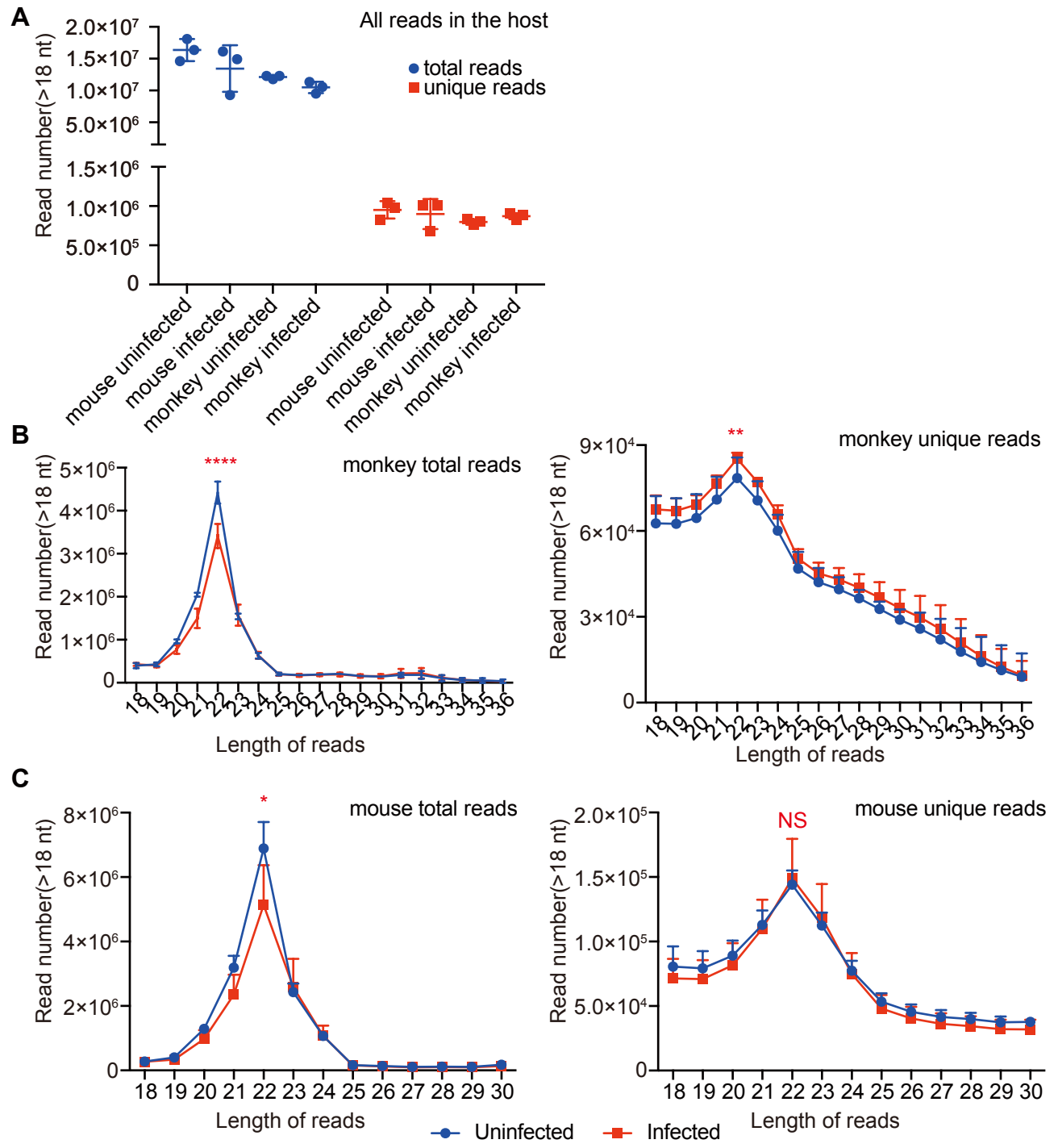
A
All reads in the host
total reads
unique reads
Read number(>18 nt)
2.0×10^7
1.5×10^7
1.0×10^7
5.0×10^6
1.5×10^6
1.0×10^6
5.0×10^5
0
mouse uninfected
mouse infected
monkey uninfected
monkey infected
mouse uninfected
mouse infected
monkey uninfected
monkey infected
B
monkey total reads
****
Read number(>18 nt)
5×10^6
4×10^6
3×10^6
2×10^6
1×10^6
0
Length of reads
monkey unique reads
**
9×10^4
6×10^4
3×10^4
0
Length of reads
C
mouse total reads
*
Read number(>18 nt)
8×10^6
6×10^6
4×10^6
2×10^6
0
18 19 20 21 22 23 24 25 26 27 28 29 30
Length of reads
mouse unique reads
NS
Read number(>18 nt)
2.0×10^5
1.5×10^5
1.0×10^5
5.0×10^4
0
18 19 20 21 22 23 24 25 26 27 28 29 30
Length of reads
Uninfected
Infected

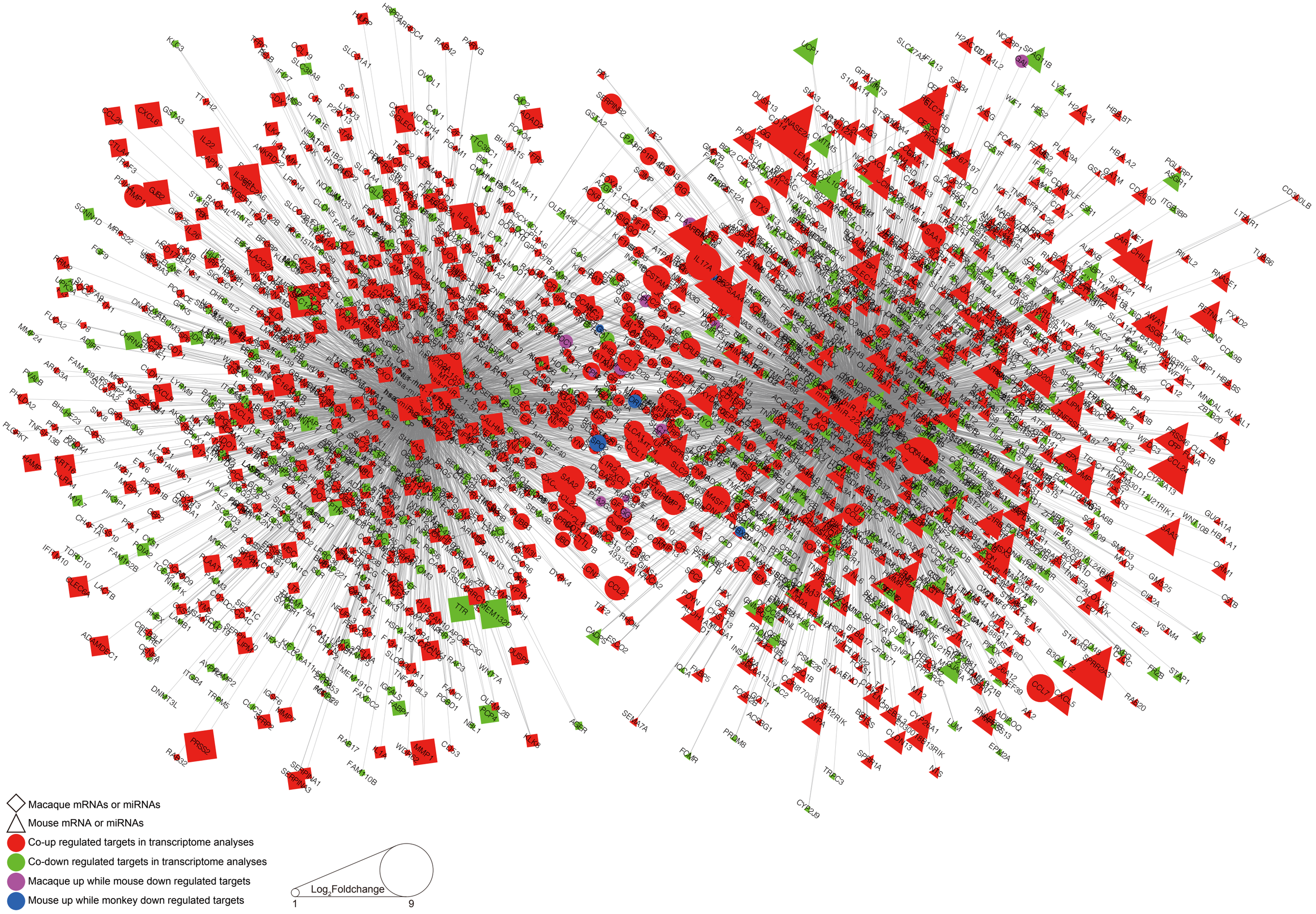
Macaque mRNAs or miRNAs
Mouse mRNA or miRNAs
Co-up regulated targets in transcriptome analyses
Co-down regulated targets in transcriptome analyses
Macaque up while mouse down regulated targets
Mouse up while monkey down regulated targets
Log2Foldchange
1
9

Viral protein interaction with cytokine and cytokine receptor
Type II diabetes mellitus
Tryptophan metabolism
Toxoplasmosis
Toll−like receptor signaling pathway
TNF signaling pathway
Tight junction
T cell receptor signaling pathway
Small cell lung cancer
Rheumatoid arthritis
Proteoglycans in cancer
Prostate cancer
Progesterone−mediated oocyte maturation
PI3K−Akt signaling pathway
Pertussis
Pathways in cancer
Parathyroid hormone synthesis secretion and action
Pancreatic secretion
p53 signaling pathway
Osteoclast differentiation
Oocyte meiosis
Non−small cell lung cancer
Non−alcoholic fatty liver disease NAFLD
NOD−like receptor signaling pathway
NF−kappa B signaling pathway
Neurotrophin signaling pathway
MicroRNAs in cancer
Melanoma
Malaria
Lysosome
Legionellosis
Kaposi sarcoma−associated herpesvirus infection
JAK−STAT signaling pathway
Influenza A
IL−17 signaling pathway
Human T−cell leukemia virus 1 infection
Human cytomegalovirus infection
HIF−1 signaling pathway
Herpes simplex infection
Hepatitis C
Ferroptosis
Epstein−Barr virus infection
Endometrial cancer
Cytokine−cytokine receptor interaction
Complement and coagulation cascades
Chemokine signaling pathway
Chagas disease American trypanosomiasis
Chagas disease
Cell cycle
Cell adhesion molecules
C−type lectin receptor signaling pathway
Bladder cancer
B cell receptor signaling pathway
Arachidonic acid metabolism
Apoptosis
Antigen processing and presentation
Amoebiasis
miRNA
Target
p value
0.05
0.04
0.03
0.02
0.01
DEGs
2
5
10
15
20
25

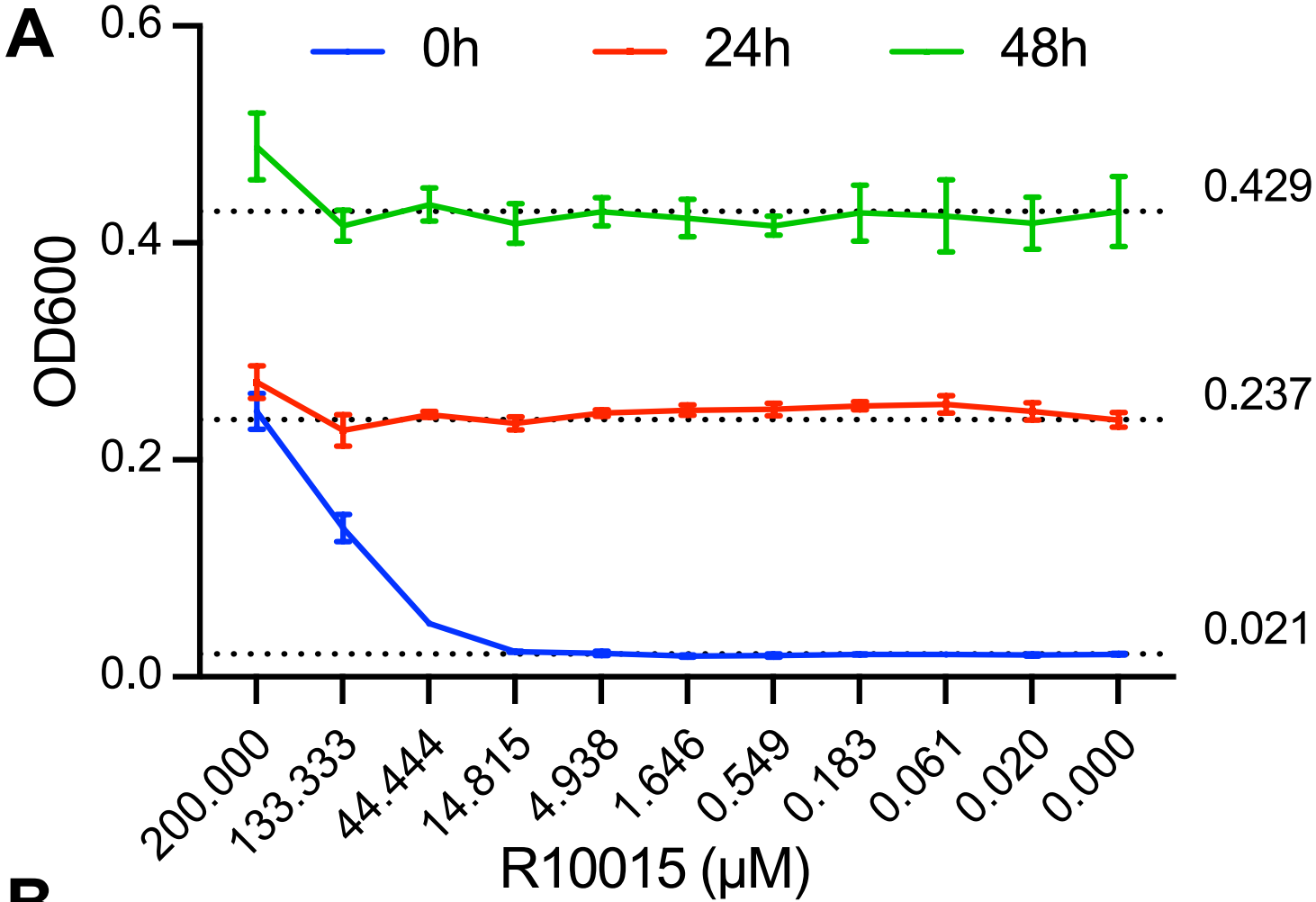
A
0h
24h
48h
OD600
0.6
0.4
0.2
0.0
0.429
0.237
0.021
200.000
133.333
44.444
14.815
4.938
1.646
0.549
0.183
0.061
0.020
0.000
R10015 (μM)

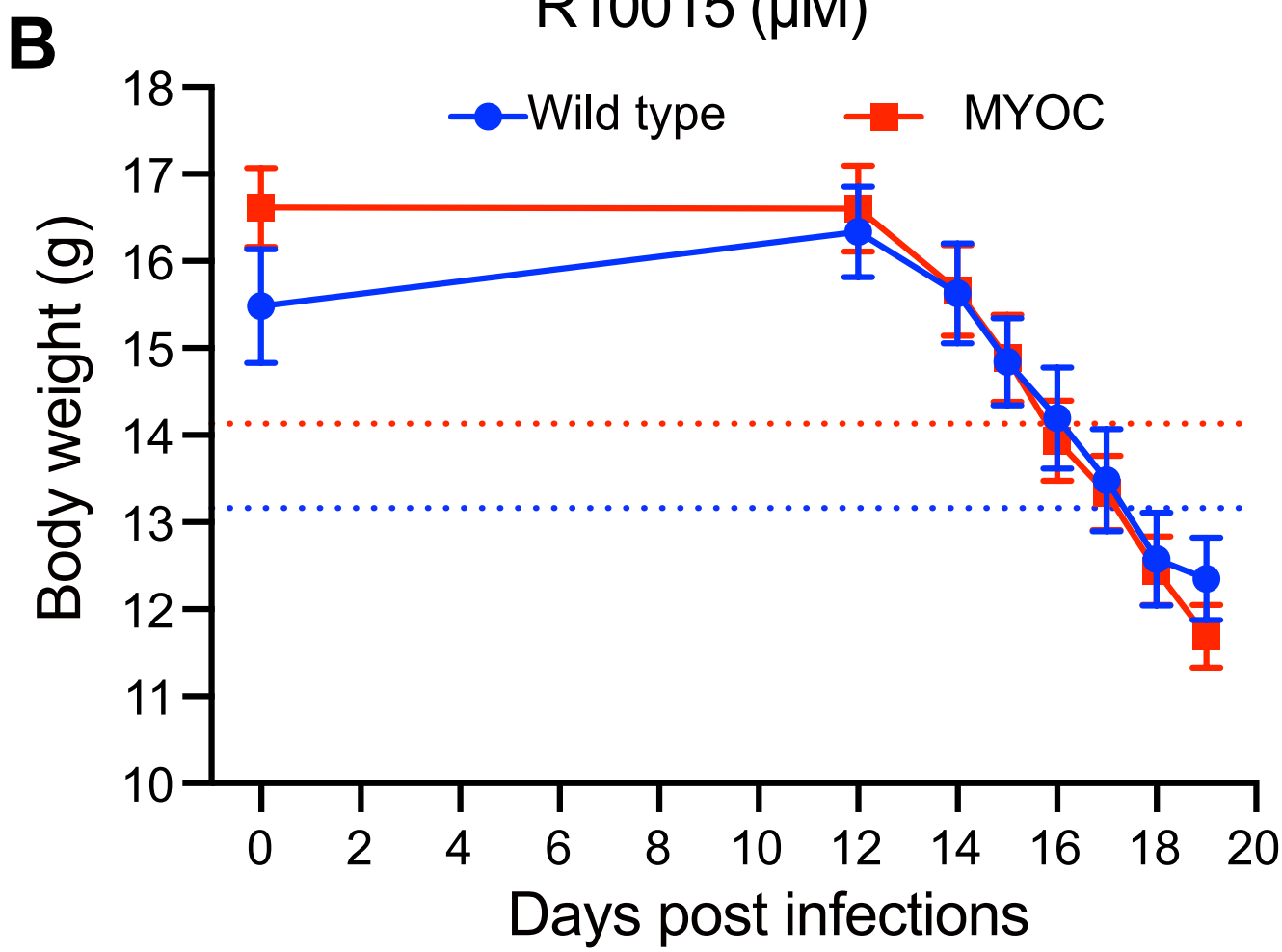
B
Wild type
MYOC
Body weight (g)
18
17
16
15
14
13
12
11
10
0
2
4
6
8
10
12
14
16
18
20
Days post infections